Experimental Mechanics
DOI 10.1007/s11340-012-9706-1

Multi-Scale Experiments and Interfacial Mechanical Modeling of Carbon Nanotube Fiber

W.-L. Deng · W. Qiu · Q. Li · Y.-L. Kang · J.-G. Guo · Y.-L. Li · S.-S. Han

Received: 28 June 2012 / Accepted: 17 December 2012

Abstract The multi-scale deformation and interfacial mechanical behavior of carbon nanotube fibers with multi-level structures are investigated by experimental and theoretical methods. Multi-scale experiments including uniaxial tensile testing, *in situ* Raman spectroscopy, and scanning electron microscopy are conducted to measure the mechanical response of multi-level structures within the fiber under tension. A two-level interfacial mechanical model is then presented to analyze the interfacial bonding strength of mesoscopic bundles and microscopic nanotubes. The evolution characteristics of multi-scale deformation of the fiber are described based on experimental characterization and interfacial strength analysis. The strengthening mechanism of the fiber is further studied. Comprehensive analysis shows that the property of multi-level interfaces is a critical factor for the fiber strength and toughness. Finally, the method of improving the mechanical properties of fiber-based materials is discussed. The result can be used to guide multi-level interface engineering of carbon nanotube fibers and fiber-based composites to produce high performance materials.

Keywords Carbon nanotube fiber · Multi-scale experiments · Multi-level structures · Interfacial mechanical model · Raman spectroscopy

W.-L. Deng · W. Qiu · Q. Li · Y.-L. Kang (✉) · J.-G. Guo
Tianjin Key Laboratory of Modern Engineering Mechanics, School of Mechanical Engineering, Tianjin University, Tianjin 300072, China
e-mail: tju_ylkang@yahoo.com.cn

Q. Li
Tianjin Key Laboratory of High Speed Cutting and Precision Machining, Tianjin University of Technology and Education, Tianjin 300222, China

J.-G. Guo
School of Engineering, Brown University, Providence, RI 02912, USA

Y.-L. Li · S.-S. Han
Key Laboratory of Advanced Ceramics and Machining Technology, Ministry of Education, School of Materials Science and Engineering, Tianjin University, Tianjin 300072, China

Introduction

Carbon nanotube (CNT) fibers exhibit high mechanical properties and possess good thermal and electrical conductivity [1, 2], that indicate potential as multi-functional materials. Studying the strengthening and toughening mechanisms of CNT fibers is critical to the future applications of fibers and fiber-based composites.

CNT fibers are characterized by multi-level structures including macroscopic fiber, mesoscopic bundle networks, and microscopic nanotubes. Many studies have shown that the multi-level structures and interfacial load transfer directly influence the macro-mechanical performance of these fibers. Jia et al. [3] studied the effect of nanotube structures on tensile properties of CNT fibers and pointed out that thinner wall thickness, smaller tube diameter, and longer tube length increased the fiber strength. Motta et al. [4] found that collapsed nanotube structures with large diameters increased the contact area between neighboring nanotubes compared with round ones, thereby improving the load transfer efficiency and forming high-performance fibers. Boncel et al. [5] reported that the reinforcement of inter-bundle interfaces by chemical treatment increased the strength and toughness of the fiber. In addition, some studies demonstrated that the inter-bundle interaction could be enhanced by making better oriented bundle networks or closely packed structures through post-spin treatments, such as twisting [6, 7] and solvent densification [8].

Published online: 03 January 2013

Theoretical simulations [9–12] are effective methods to study the interfacial load transfer of nanotubes. Qian et al. [11] found through molecular simulations that surface tension and inter-tube corrugation were the two major factors in inter-tube load transfer. Zhang et al. [12] investigated the pressure effect on interfacial friction within CNT bundles and found that the friction increased four times when the pressure applied to the bundle was beyond a critical value. Meanwhile, progress has been made in experimental investigation of mechanical properties of CNT fibers. For example, based on the Raman stress sensitivity of CNTs, Raman spectroscopy was used to study the deformation behavior of CNT fibers. From Raman testing, Ma et al. [13] suggested that the strength of CNT macroarchitectures was controlled by the strength of inter-bundle junctions. By Raman and X-ray diffraction measurements, Vilatela et al. [14] identified the non-uniform load transfer between bundles as the major factor limiting the fiber strength. Li et al. [15] investigated the deformation mechanism of CNT fibers using Raman spectroscopy and implied that the strength was related to internal interfaces. However, in-depth understanding of the role of interfaces in fiber deformation as yet remains elusive. Thus, there is a need to investigate the relationship between strength/toughness and multi-level structures as well as interfaces if fiber mechanical performance is to be improved.

In this paper, the structural deformation and interfacial mechanical behavior of CNT fibers are investigated. To begin, multi-scale experiments including macroscopic uniaxial tensile testing, microscopic Raman spectroscopy, and mesoscopic scanning electron microscopy (SEM) are used to measure the mechanical response of multi-level structures under tension. A two-level interfacial mechanical model is then presented that is used to analyze the interfacial bonding strength at the bundle and nanotube levels. Next, the characteristics of multi-scale deformation of the fiber are described based on the experimental and theoretical analysis. Finally, the relationship between fiber strength/toughness and interfacial properties is discussed.

CNT Fiber and Principle of Raman Measurement

CNT Fiber with Multi-Level Structures

The CNT fibers used for this study were prepared from the chemical vapor deposition (CVD) aerogel process [2], with diameters typically in the range of 130–150 μm (Fig. 1(a)). The mesoscopic structure of the fiber consists of relatively thick, straight bundles and fine, curly threads preferentially aligned along the fiber axis (see the SEM image of Fig. 1(b)). The bundles and threads have diameters ranging from 30 to 100 nm. Transmission electron microscopy (TEM) images (Fig. 1(c, d)) show the microscale structure of the fiber. The CNTs within bundles (threads) are double-walled and their diameters are approximately 8 to 10 nm. Owing to their large diameters, these double-walled nanotubes (DWNTs) appear flattened with a "dog-bone" cross-section [16] (Fig. 1(d)).

CNT fibers are featured by multi-level structures (Fig. 2). At the bundle level, the straight and thick bundles filled with fine, curly threads constitute mesoscopic networks with preferential alignment along the fiber axis (Fig. 2(b)), At the nanotube level, the microscopic structure is composed of flattened DWNTs that are closely stacked into bundles and threads, similar to graphitic layer stacks (Fig. 2(c)). Therefore, interfacial contact and load transfer in the fiber occur between both the mesoscopic bundles/threads and the microscopic nanotubes.

Principle of Raman Measurement for CNTs

In recent years, Raman spectroscopy has been effectively applied in experimental mechanical measurements [17–22]. Raman scattering is sensitive to the interatomic distance and the Raman band frequency shifts with strain that is applied to Raman-active materials. For CNTs, the strain exerted on nanotubes extends or shortens the C−C bond, causing Raman shift in the spectrum [23, 24]. The common Raman signatures of CNTs include the so-called radical breathing mode (RBMs) bands, the graphite (G) band, the disorder-induced (D) band, and its overtone (G′) band. Because the G′ band is the most sensitive to external stresses [24], its Raman shift, intensity, and full width at half-maximum (FWHM) were analyzed and interpreted to yield information of the deformation and interfacial mechanical behavior of the fiber. The Raman experiment was conducted on a Renishaw's inVia system and all Raman spectra were obtained under a 633 nm incident/reflected He–Ne laser light with the polarization direction parallel to the fiber axis. Raman measurement was taken with a 50× objective lens and a laser spot size of 2 μm (Fig. 3(a)). The laser power was approximately 10 mW. Figure 3(b) shows a typical Raman spectrum of an unstrained fiber with well-defined D (1330.4 cm^{-1}), G (1580.8 cm^{-1}), and G′ (2652.1 cm^{-1}) bands.

Multi-Scale Experiments of CNT Fiber

Given the multi-level structural feature of CNT fibers, experiments were performed to measure the structural responses of the fiber under tension at multiple length scales. A micro-tensile loading device was used to measure the macroscopic mechanical behavior of the fiber, and Raman spectra were obtained to detect the microscopic strain in the DWNTs during fiber deformation. Meanwhile, the structural evolution of mesoscopic bundles and threads caused by tension was analyzed through SEM.

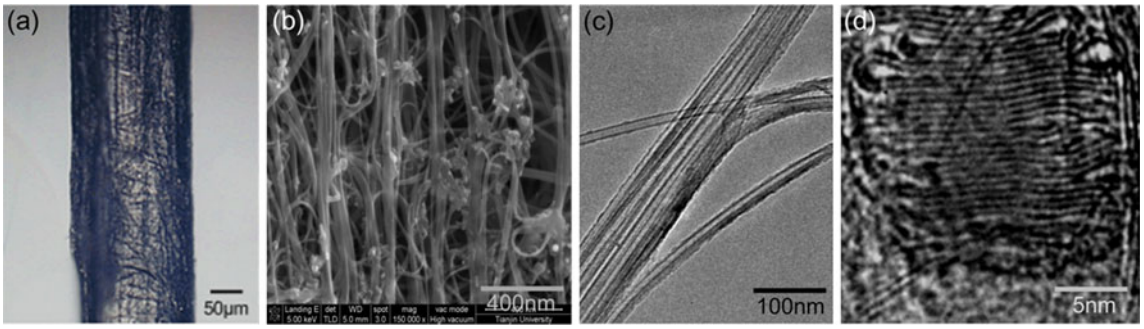

Fig. 1 Structural characterization of CNT fiber: (**a**) Optical micrograph, (**b**) SEM image showing the fiber consists of thick, straight bundles and fine, curly threads, (**c**) TEM image of bundles (*threads*), (**d**) DWNTs within bundles (*threads*) flattened with a "dog-bone" cross-section

Uniaxial Tensile Testing

The uniaxial tensile testing of single fibers was conducted on a homemade micro-loading device with 1 N load cell (Fig. 4(a)). The device is equipped with a screw displacement loader and a micro-force measuring device with precisions of up to 10 μm and 1 mN, respectively. This device can record the displacement and applied force during testing. Figure 4(b) gives a typical stress–strain curve of the fiber with a gauge length of 5 mm. The fiber undergoes three-stage deformation: (I) elastic, (II) strengthening, and (III) damage-fracture with a long strengthening process from 1.2 % to 11.8 %. The elastic modulus and ultimate strength are 15.6 GPa and 0.3 GPa, respectively. The elongation at fracture is 13.6 % and the absorbed energy per unit volume before fracture is 32.5 MJ/m^3, both indicating good fiber toughness.

In Situ Raman Measurement

To detect micromechanical information during the fiber deformation, the *in situ* Raman technique was employed to measure the spectra of DWNTs. Figure 4(b) shows a plot of frequency variation of the G′ band against fiber strain which follows a similar trend to that of the stress–strain curve. As strain is initially applied to the fiber, the peak frequency shifts linearly to low wavenumbers at a rate of 2.22 cm^{-1} per 1 % strain, indicating that DWNTs inside the fiber are stretched elastically. Cronin et al. [24] reported a downshift rate of 37.3 cm^{-1} per 1 % strain of the G′ band in individual strained SWNTs, 17 times that of the fiber used in this work. Such a low downshift rate indicates poor load transfer efficiency between bundles. The fiber yields above 1.2 % strain and the stress increases slowly after yielding. Correspondingly, the downshift rate decreases to only 0.055 cm^{-1} per 1 % strain. When the fiber fractures, the G′ band frequency almost recovers to its initial value. This result indicates that the strain of DWNTs nearly disappears after the fiber break.

The ratio of the D and G band intensities (I_D/I_G) is related to the number of defects and bond damage within individual CNTs [25]. Table 1 shows the I_D/I_G values at the unstrained, elastic (1.2 %), strengthening (5.2 %), and fractured (13.6 %) stages. These values remain almost constant around 0.24, which indicates no obvious damage or breaking of C-C bond in DWNTs during tensile deformation.

Figure 4(b, c) plot the changes of FWHM and intensity of the G′ band against fiber strain, respectively. The FWHM increases with fiber strain, then plateaus, and finally recovers to almost its initial value after the fiber has fractured. The intensity, however, shows an overall increasing trend indicating a general enhancement in the alignment of DWNTs along the fiber axis. In addition, the peak shape of the G′ band is asymmetrically broadened, as seen in Fig. 4(d), which depicts three different spectral curves of the undeformed, 1.2 %- and 10.8 %-strained fiber. With increasing

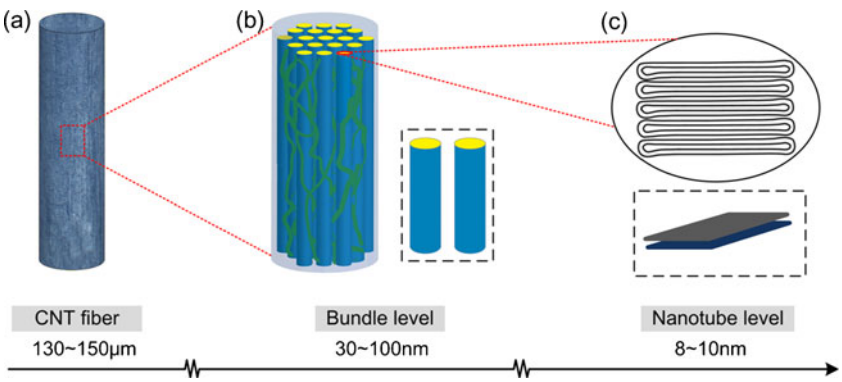

Fig. 2 Multi-level structural model of CNT fiber: (**a**) Macroscopic fiber, (**b**) Mesoscopic bundle and thread networks, (**c**) Microscopic flattened DWNTs; the schematics enclosed by *dashed lines* in (**b**) and (**c**) indicate the interfacial contacts between parallel bundles and between DWNT walls, respectively

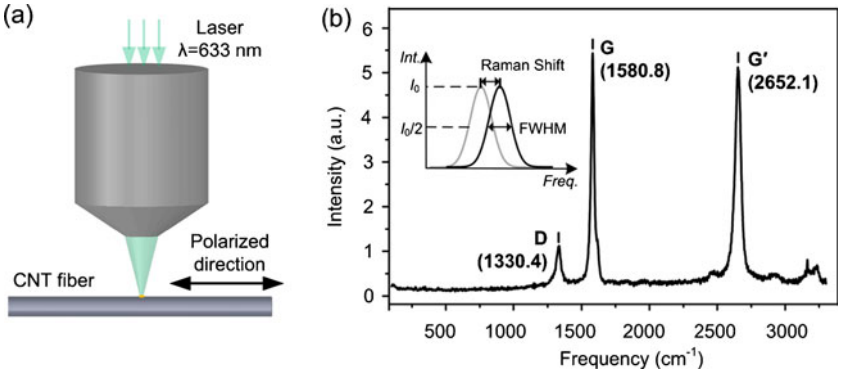

Fig. 3 (**a**) Schematic of Raman experiment, (**b**) A typical Raman spectrum of the fiber with the well-defined D, G, and G′ bands, the inset in (**b**) illustrates parameters of the Raman band such as Raman shift, intensity, and FWHM

strain, the high-wavenumber edge of Raman spectra remains almost unmoved; but the low-wavenumber edge shows an evident shift to lower wavenumbers. This result suggests that non-uniform load sharing occurs during fiber deformation. Asymmetrical broadening of the Raman spectrum has also been observed in strained CNT macrostructures [13] and composites [26] under uniaxial loading, which is related to the inhomogeneous stress distribution in materials.

SEM Observation

The structural evolution of the fiber before and after fracture was investigated by SEM imaging. The fracture morphology (Fig. 5(a)) reveals that the failure path is not uniform but composed of many minute bundles pulled out along the fracture. The failure mode clearly suggests that the fiber fracture is ductile, rather than brittle, caused through interfacial damage. To understand better the structure changes in the fiber, microstructures of the fracture tip (point A) and a point 500 μm away from the fracture (point B) are studied. The SEM image of point A (Fig. 5(b)) shows that the bundles and threads are not only straightened along the fiber axis, but also thinned to an average diameter of ~21 nm, compared with the average diameter of ~29 nm of unstrained structures. However, no significant changes are observed in the diameter of bundles and threads at point B (Fig. 5(c)). The structure difference between points A and B is strong evidence of slipping that occurs between DWNTs within bundles and threads.

Interfacial Mechanical Modeling Analysis

As is evident from multi-scale experiments, interfaces between both bundles and nanotubes play an important role in fiber deformation, and the interfacial slipping finally results

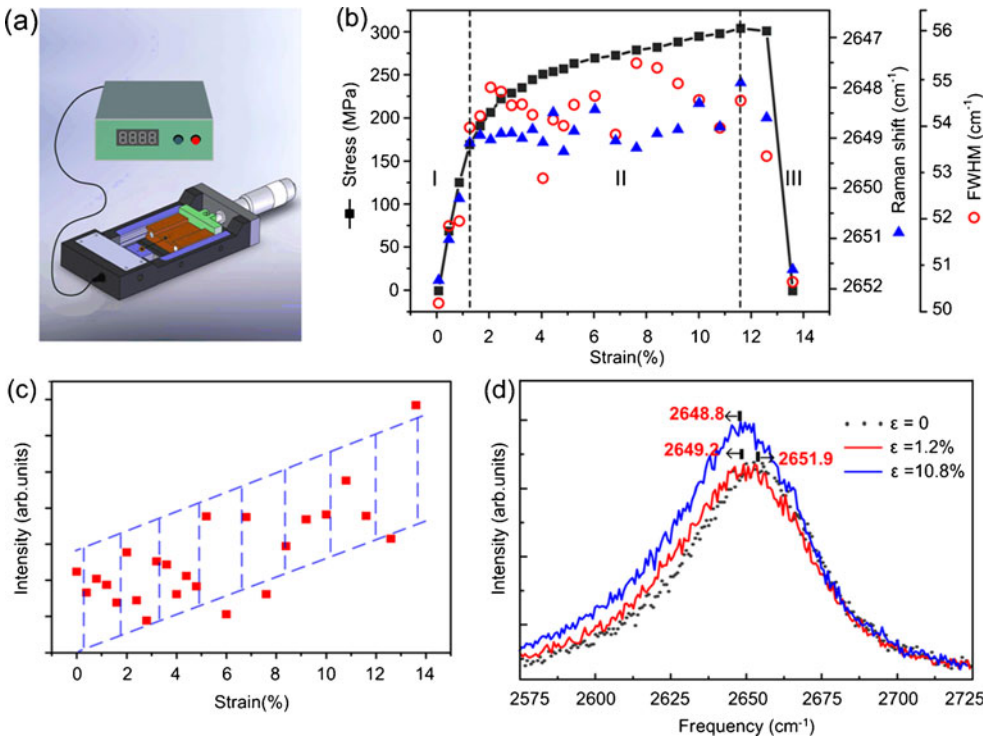

Fig. 4 (**a**) Micro-loading device, (**b**) Stress–strain curve of a CNT fiber under tensile deformation (*squares*), variations of Raman shift (*triangles*) and FWHM (*circles*) of the G′ band as a function of fiber strain, (**c**) Raman intensity of the G′ band against fiber strain, (**d**) Raman spectra of the G′ band at different fiber strains showing asymmetrical broadening at lower wavenumbers

Table 1 Ratios of the D and G band intensities (I_D/I_G) at different strains

Strain (%)	0	1.2	5.2	13.6
I_D/I_G	0.241	0.243	0.243	0.243

in fiber failure. Thus, a study of slipping of multi-level interfaces at different stages is necessary in analyzing the deformation mechanism of the fiber. In this section, a two-level interfacial mechanical model is developed to compare the interfacial strengths of mesoscopic bundles and microscopic nanotubes.

At the mesoscale, the bundles are simplified as cylinders with diameter r (Fig. 6(a)). The interfacial bonding of bundles is considered to originate from weak van der Waals interactions. The van der Waals force between two parallel bundles is [27]

$$F_{bundle} = \frac{AL_b r^{1/2}}{16 d_0^{5/2}}, \tag{1}$$

where A is the Hamaker constant with L_b and d_0 the respective contact length and separation distance of the bundles. The shear stress arises from interfacial friction and the interfacial strength is equal to the maximum static friction. Thus, the interfacial strength at the bundle level is

$$\tau^m_{bundle} = \frac{\mu \cdot F_{bundle}}{w_e L_b} = \frac{\mu A r^{1/2}}{16 w_e d_0^{5/2}}, \tag{2}$$

where μ is the friction coefficient. The effective contact width, w_e, is defined as the width within which the gap between two bundles is less than or equal to $3d_0$. Thus, $w_e = 2\sqrt{r^2 - (r - d_0)^2}$.

At the microscale, the flattened DWNT stacks within bundles are similar to regular graphitic layers. Therefore, the nanotube walls are simplified as planks with thickness t (Fig. 6(b)). The van der Waals force between two faced planks is [27]

$$F_{tube} = \frac{AwL_c}{6\pi}\left(\frac{1}{d^3} - \frac{2}{(d+t)^3} + \frac{1}{(d+2t)^3}\right), \tag{3}$$

where L_c is the length of DWNTs with w and d the respective width and gap of DWNT stacks. Similarly, the interfacial strength at the nanotube level is

$$\tau^m_{tube} = \frac{\mu' \cdot F_{tube}}{wL_c} = \frac{\mu' A}{6\pi}\left(\frac{1}{d^3} - \frac{2}{(d+t)^3} + \frac{1}{(d+2t)^3}\right), \tag{4}$$

where μ' is the friction coefficient of the nanotube walls.

Therefore, the ratio of these two interfacial strengths is

$$\alpha = \frac{\tau^m_{bundle}}{\tau^m_{tube}} = \frac{3\pi\mu r^{1/2}}{8\mu' w_e d_0^{5/2}}\left(\frac{1}{d^3} - \frac{2}{(d+t)^3} + \frac{1}{(d+2t)^3}\right)^{-1}. \tag{5}$$

By combining SEM/TEM images, the ranges of radius r and distance between bundles d_0 are determined to be 15 to 50 nm and 0.5 to 1 nm, respectively. The thickness of nanotube walls t is equal to the intra-tube distance of DWNTs, *i.e.*, d is 0.35 nm [28, 29]. The friction coefficients for nanotubes and for bundles are the same. Subsequently, the interfacial strength ratio α is between 0.03 and 0.27. The analysis suggests that the mesoscopic interface between bundles is weaker than the microscopic interface between DWNTs. Therefore, the weaker interface in the fiber is identified and slipping beyond a critical load will first occur at the inter-bundle interfaces.

Multi-Scale Deformation Mechanism of CNT Fiber

Based on the experimental results and interfacial modeling analysis, the deformation mechanism of CNT fibers is

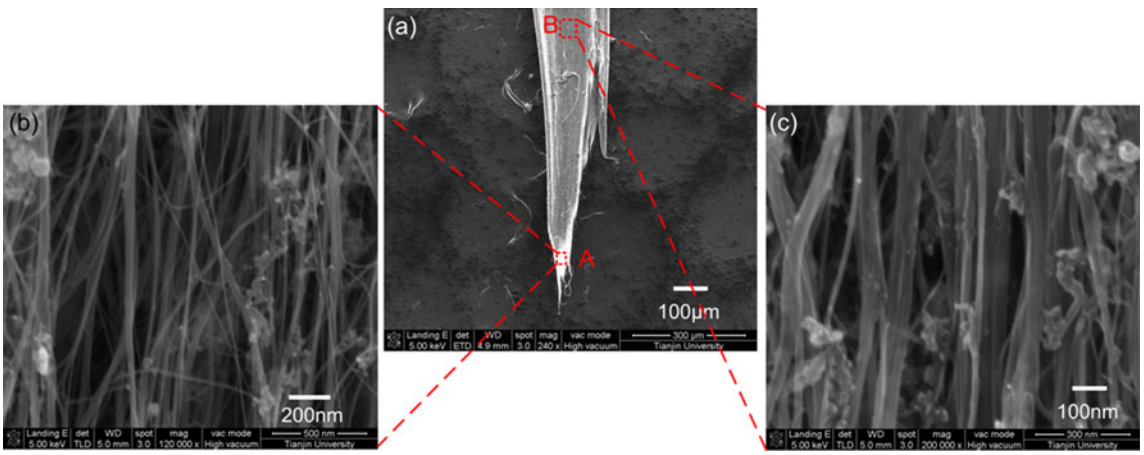

Fig. 5 (**a**) SEM image of fracture morphology of the fiber, (**b**) and (**c**) are SEM images of the microstructures at the fracture tip and at a point 500 μm away from the fracture, respectively

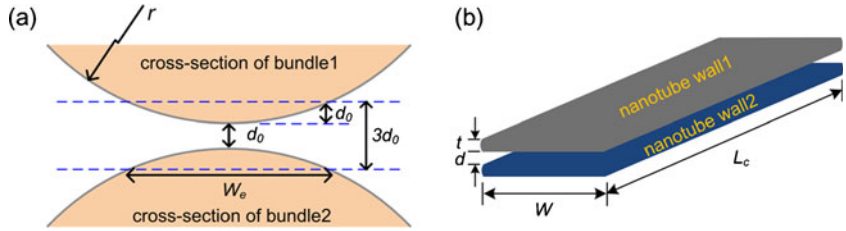

Fig. 6 Schematic of interfacial bonding strength analysis (**a**) between two bundles (cross-sectional view) and (**b**) between two nanotube walls

described as follows. At the elastic stage, most of the load is initially carried by straight bundles. Deformation of the nanotubes in these bundles increases linearly with the applied load. The curly threads are gradually stretched but their internal nanotubes bear very little of the load. The average stress of nanotubes increases with fiber strain, which is consistent with the downshift of the G' band. However, load sharing within the fiber is non-uniform because the load borne by the nanotubes in bundles gradually increases whereas the nanotubes in threads are subjected to little of the load.

As the strain increases, parts of the bundles are overloaded. The interfacial shear stress arises and finally exceeds the interfacial strength. Slipping occurs initially at the bundle level due to the weaker inter-bundle interfaces, which leads to yielding of the fiber. Meanwhile, the curly thin threads are gradually straightened to bear some of the load. At this stage, the fiber stress increases slowly and shows strain strengthening. The strengthening behavior arises from the gradual bearing process of threads and the frictional resistive force between inter-bundle interfaces.

Although more curly threads are involved in load bearing, interfacial damage continuously accumulates and leads to stress redistribution within the fiber up until the end of strengthening stage. As reflected in the asymmetrical broadening of the peak shape of the G' band, the degree of local stress concentration becomes increasingly severe, causing the DWNTs in bundles and threads to slide with respect to one another, as evident in the SEM images (Fig. 5). It should be noted that some nanotubes are not strictly stacked into bundles and threads; but several flattened nanotubes group together to form a sub-bundle and those sub-bundles constitute a bundle (thread). Slipping may also take place between sub-bundles. Thus, interfacial slipping at meso- and micro-scales collectively accelerates the stress redistribution in the fiber, promotes the micro-crack propagation, and finally leads to the fiber fracture.

Overall, the mechanical behavior of CNT fibers is closely correlated with multi-level structures and interfaces. The evolution characteristics of multi-scale deformation of the fiber during three different stages are shown in Fig. 7.

Discussions and Conclusion

The present work shows that synergetic measurement combining macro tensile testing, *in situ* micro-Raman spectroscopy, and SEM is an effective method for experimental mechanics that can provide deformation characteristics of material at different structural levels, and thus for multi-scale mechanical analysis.

Through multi-scale experiments, deformation and strengthening mechanisms of the CNT fiber with multi-level structures were described along with interfacial modeling

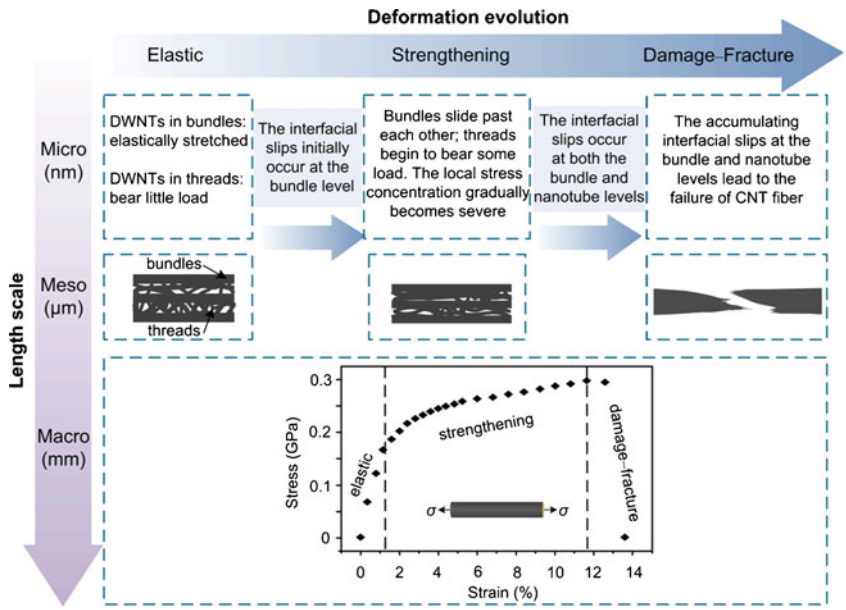

Fig. 7 Evolution characteristics of multi-scale deformation of the fiber during three different stages under tension

to provide a mechanical analysis. Interfacial slipping causes the transitions between different fiber deformation stages and multi-level interfacial properties are the main factors affecting the fiber strength and toughness. First, the yield after elastic stage is related to the interfacial slipping between mesoscopic bundles; thus the yield strength can be enhanced by improving interfacial bonding at the bundle level. Second, fiber strengthening arises from the gradual load bearing in curly threads and the interfacial friction between bundles, which can be reinforced through twisting fibers to reduce the distance between bundles or by infiltrating polymers as an interfacial phase. Finally, interfacial slipping of mesoscopic bundles and microscopic nanotubes contributes together to the local stress concentration and results in fiber damage and fracture. The improvement of multi-level interfacial properties should be conducted to increase fiber performance.

The comprehensive analysis also provides inspiration in the design of CNT fibers and composites with high strength and toughness. Because interfacial properties play a significant role in mechanical properties of the material, the weak interfacial bonding should be enhanced to avoid premature slipping at the interface and thus to obtain high strength. Furthermore, the frictional resistive force can be reinforced by adding a flexible interfacial phase into the material with the intent to improve the toughness when interfacial failure occurs.

Acknowledgments The authors acknowledge the financial support of this work provided by the National Basic Research Program of China (No. 2012CB937500), the National Natural Science Foundation of China (No. 11002097), and the Key Grant of Chinese Ministry of Education (No.309010).

References

1. Koziol K, Vilatela J, Moisala A, Motta M, Cunniff P, Sennett M, Windle A (2007) High-performance carbon nanotube fiber. Science 318:1892–1895. doi:10.1126/science.1147635
2. Zhong XH, Li YL, Liu YK, Qiao XH, Feng Y, Liang J, Jin J, Zhu L, Hou F, Li JY (2010) Continuous multilayered carbon nanotube yarns. Adv Mater 22:692–696. doi:10.1002/adma.200902943
3. Jia JJ, Zhao JN, Xu G, Di JT, Yong ZZ, Tao YY, Fang C, Zhang ZG, Zhang XH, Zheng LX, Li QW (2011) A comparison of the mechanical properties of fibers spun from different carbon nanotubes. Carbon 49:1333–1339. doi:10.1016/j.carbon.2010.11.054
4. Motta M, Moisala A, Kinloch IA, Windle AH (2007) High performance fibres from 'dog bone' carbon nanotubes. Adv Mater 19:3721–3726. doi:10.1002/adma.200700516
5. Boncel S, Sundaram RM, Windle AH, Koziol KKK (2011) Enhancement of the mechanical properties of directly spun CNT fibres by chemical treatment. ACS Nano 5(12):9339–9344. doi:10.1021/nn202685x
6. Cheng TW, Hsu WK (2007) Winding of single-walled carbon nanotube ropes: an effective load transfer. Appl Phys Lett 90 (12):123102. doi:10.1063/1.2714282
7. Rong Q, Wang J, Kang Y, Li Y, Qin Q (2012) A damage mechanics model for twisted CNT fiber. Acta Mech Solida Sinica 25(4):342–347
8. Liu K, Sun YH, Zhou RF, Zhu HY, Wang JP, Liu L, Fan SH, Jiang KL (2010) Carbon nanotube yarns with high tensile strength made by a twisting and shrinking method. Nanotechnology 21:045708. doi:10.1088/0957-4484/21/4/045708
9. Zhou LJ, Kang YL, Guo JG (2011) Phenomenological model of interfacial stress transfer in carbon nanotube reinforced composites with van der Waals effects. Polym Compos 32(7):1069–1076. doi:10.1002/pc.21124
10. Li C, Liu Y, Yao X, Ito M, Noguchi T, Zheng Q (2010) Interfacial shear strengths between carbon nanotubes. Nanotechnology 21 (11):115704. doi:10.1088/0957-4484/21/11/115704
11. Qian D, Liu WK, Ruoff RS (2003) Load transfer mechanism in carbon nanotube ropes. Compos Sci Technol 63(11):1561–1569. doi:10.1016/s0266-3538(03)00064-2
12. Zhang X, Li Q (2009) Enhancement of friction between carbon nanotubes: an efficient strategy to strengthen fibers. ACS Nano 4 (1):312–316. doi:10.1021/nn901515j
13. Ma W, Liu L, Yang R, Zhang T, Zhang Z, Song L, Ren Y, Shen J, Niu Z, Zhou W, Xie S (2009) Monitoring micromechanical process in macroscale carbon nanotube films and fibers. Adv Mater 21 (5):603–608. doi:10.1002/adma.200801335
14. Vilatela JJ, Deng L, Kinloch IA, Young RJ, Windle AH (2011) Structure of and stress transfer in fibres spun from carbon nanotubes produced by chemical vapour deposition. Carbon 49 (13):4149–4158. doi:10.1016/j.carbon.2011.05.045
15. Li Q, Kang YL, Qiu W, Li YL, Huang GY, Guo JG, Deng WL, Zhong XH (2011) Deformation mechanisms of carbon nanotube fibres under tensile loading by *in-situ* Raman spectroscopy analysis. Nanotechnology 22(22):225704. doi:10.1088/0957-4484/22/22/225704
16. Elliott J, Sandler J, Windle A, Young R, Shaffer M (2004) Collapse of single-wall carbon nanotubes is diameter dependent. Phys Rev Lett 92(9):095501. doi:10.1103/PhysRevLett.92.095501
17. Kang YL, Qiu Y, Lei ZK, Hu M (2005) An application of Raman spectroscopy on the measurement of residual stress in porous silicon. Opt Lasers Eng 43(8):847–855. doi:10.1016/j.optlaseng.2004.09.005
18. Qiu W, Kang YL, Lei ZK, Qin QH, Li Q, Wang Q (2010) Experimental study of the Raman strain rosette based on the carbon nanotube strain sensor. J Raman Spectrosc 41(10):1216–1220. doi:10.1002/jrs.2584
19. Kao CC, Young RJ (2004) A Raman spectroscopic investigation of heating effects and the deformation behaviour of epoxy/SWNT composites. Compos Sci Technol 64(15 SPEC. ISS):2291–2295. doi:10.1016/j.compscitech.2004.01.019
20. Starman L, Coutu R (2012) Stress monitoring of post-processed MEMS silicon microbridge structures using Raman spectroscopy. Exp Mech. doi:10.1007/s11340-011-9586-9
21. Srikar V, Spearing S (2003) A critical review of microscale mechanical testing methods used in the design of microelectromechanical systems. Exp Mech 43(3):238–247. doi:10.1007/bf02410522
22. Arjyal B, Katerelos D, Filiou C, Galiotis C (2000) Measurement and modeling of stress concentration around a circular notch. Exp Mech 40(3):248–255. doi:10.1007/bf02327496
23. Kumar R, Cronin SB (2007) Raman scattering of carbon nanotube bundles under axial strain and strain-induced debundling. Phys Rev B 75:155421. doi:10.1103/PhysRevB.75.155421
24. Cronin SB, Swan AK, Ünlü MS, Goldberg BB, Dresselhaus MS, Tinkham M (2005) Resonant Raman spectroscopy of individual metallic and semiconducting single-wall carbon nanotubes under uniaxial strain. Phys Rev B 72:035425. doi:10.1103/PhysRevB.72.035425
25. Dresselhaus MS, Jorio A, Souza Filho AG, Saito R (2010) Defect characterization in graphene and carbon nanotubes using Raman spectroscopy. Phil Trans R Soc A Math Phys Eng Sci 368 (1932):5355–5377. doi:10.1098/rsta.2010.0213

26. Nikolaev P, Menamparambath MM, Boul PJ, Moloney P, Arepalli S (2011) Raman probing of adhesion loss in carbon nanotube – reinforced composite. Compos Part A 42:1681–1686. doi:10.1016/j.compositesa.2011.07.022
27. Parsegian VA (2006) Van der Waals forces: a handbook for biologists, chemists, engineers, and physicists. Cambridge University Press, New York
28. Cai J, Wang CY, Yu T, Yu S (2009) Wall thickness of single-walled carbon nanotubes and its Young's modulus. Phys Scr 79(2):025702. doi:10.1088/0031-8949/79/02/025702
29. Li C, Chou TW (2003) A structural mechanics approach for the analysis of carbon nanotubes. Int J Solids Struct 40(10):2487–2499. doi:10.1016/s0020-7683(03)00056-8